

Design and Analysis of an Electrical Variable Transmission for a Series-Parallel Hybrid Electric Vehicle

Li Chen, Futang Zhu, Minmin Zhang, Yi Huo,
Chengliang Yin, and Hui Peng

Abstract—This paper describes the mathematical modeling, analysis, and simulation results of a novel electrical variable transmission (EVT) for a series-parallel hybrid electric vehicle (SPHEV). The proposed EVT uses a two-degree-of-freedom (2-DOF) planetary gearset with four clutches to combine an engine and two electric machines with the vehicle. The topology of the planetary gearset is the same as that of conventional four-speed automatic transmissions. Therefore, the proposed EVT can be mass-produced and quite easily packaged. Nine operation modes can be realized. The properly arranged clutches more flexibly transmit power flow and avoid high spin losses for the engine and electric machines. Simulation under the New European Driving Cycle (NEDC) drive cycle shows that the fuel consumption of the proposed SPHEV is 5.62% lower than a benchmark vehicle, which uses two planetary gearsets and no clutches, indicating the fuel economy potential of this concept. The life cycle of the electric machines is expected to be extended, because the open or locked operations of the clutches allow efficient operation and, thus, might reduce the chance of overheating. Finally, the speed range of the electric machines is found to be smaller, compared with that used in the benchmark vehicle, which implies ease of manufacture, good sustainability, and low cost.

Index Terms—Electrical variable transmission (EVT), modeling, planetary gearset, series-parallel hybrid electric vehicle (SPHEV).

I. INTRODUCTION

Hybrid electric vehicles (HEVs), using an engine and one or more electric machines, are widely regarded as the most promising solution for clean vehicles in the short term to midterm [1]. Series-parallel HEVs (SPHEVs) can take advantage of the positive attributes of both series and parallel HEVs and are dominating the current passenger HEV market. An SPHEV requires a transmission device to couple the engine and electric machines with the vehicle. For hybrid vehicles, the coupling mechanism must be compact, efficient, easy to control, and of low cost.

Recently, various two-degrees-of-freedom (2-DoF) devices for the SPHEV were studied. They are known as electrical variable transmissions (EVTs) [2]. A typical design is the Toyota Hybrid System (THS) [3], which uses a 2-DoF planetary gearset to couple the engine and two electric machines. The engine speed and torque can be freely assigned by manipulating the two electric machines [4]. Therefore, EVT's can narrow engine operating points to be within an efficient

region, regardless of vehicle speeds, achieving superior performance using a relatively simple transmission design.

The 2-DoF EVT's can be realized through various combinations of planetary gearsets [5]. The THS is on the extreme end of hardware simplicity, using only one planetary gear and no clutches in the power flow, as shown in Fig. 1(a). As a result of the simple mechanical design, the electric machines are required to operate at a wide range of speeds. For example, the THS generator speed is up to 10 000 r/min [3]. To obtain large torque, Fig. 1(b) shows improved THS, which uses an extra planetary gearset as a reduction gear to connect an electric machine. The maximum speed of the electric machine is up to 13 900 r/min, and the maximum torque is up to 207 N · m [6]. These specifications lead to the need for more expensive motors and other components such as bearings. Another disadvantage, due to the clutchless design, is higher spin losses, even when no torque is generated by a power device.

EVT with properly arranged clutches can avoid the above deficiencies. Through clutch engagement and disengagement, EVT's can more flexibly and efficiently transmit power flow. A variety of EVT's with clutches have been put forth by GM, Renault, and The Timken Company [7], [8]. GM has registered tens of patents with different designs for two-mode HEV powertrains, which contain one or two planetary gearsets and two or three clutches. One of the designs is shown in Fig. 1(c). The Renault EVT design in Fig. 1(d) has two planetary gearsets and two dog clutches. Timken's design in Fig. 1(e) has two planetary gearsets and four clutches (two rotating clutches and two braking clutches). However, due to their more complex architecture, smooth operation under various driving conditions and cost require careful analysis and complex controls.

This paper proposes a novel 2-DoF EVT, which consists of two planetary gearsets and two electric machines embedded with four clutches. The two planetary gearsets are configured in the same way as those of the popular four-speed automatic transmissions (ATs) such as GM(4L60E), CHRYSLER(42LE), ZF(4HP-18), etc. [12]. The four clutches are derived from the conventional AT with their axial shafts modified to connect the motors. With an appropriate configuration of the planetary gears and clutches, the specifications of the motors can be optimized. The proposed EVT makes use of many components of the conventional ATs, which have been refined and perfected for decades. Thus, the reliability and cost effectiveness of the proposed EVT, which reuses part of the AT, are likely to be superior to EVT's that are newly designed. We believe that the proposed architecture is more viable for practical applications because of its evolutionary nature.

In this paper, a simulation model is developed for the proposed EVT, which is used to analyze and evaluate its performance. Section II explains the configuration and design of the proposed EVT. The simulation model is given in Section III, followed by a description of the rule-based energy management strategy in Section IV. Finally, simulation results and a discussion of these results are given in Section V.

II. SYSTEM ARCHITECTURE

A. Configuration

The topology of the proposed EVT is identical to that used in several conventional four-speed ATs [12], as shown in Fig. 2(a). The EVT consists of two planetary gearsets. The carrier gear of the first planetary gearset C1 is connected to the ring gear R2 of the second planetary gearset, and the first ring gear R1 is connected to the second carrier gear C2. Five clutches are employed, three of which are rotating

Manuscript received June 17, 2010; revised November 1, 2010 and January 11, 2011; accepted February 15, 2011. Date of publication April 5, 2011; date of current version June 20, 2011. This work was supported in part by the Science and Technology Commission of Shanghai Municipality of the People's Republic of China and in part by Shanghai Automobile Gear Works under Grant 07dz11501. The review of this paper was coordinated by Mr. D. Diallo.

L. Chen, F. Zhu, and C. Yin are with the School of Mechanical Engineering, Shanghai Jiao Tong University, Shanghai 200240, China (e-mail: li.h.chen@sjtu.edu.cn).

M. Zhang is with the School of Mechanical Engineering and Materials Science, University of Pittsburgh, Pittsburgh, PA 15213 USA.

Y. Huo is with United Automotive Electronic System Company, Ltd. Shanghai 201206, China.

H. Peng is with the Department of Mechanical Engineering, University of Michigan, MI 48109 USA (e-mail: hpeng@umich.edu).

Color versions of one or more of the figures in this paper are available online at <http://ieeexplore.ieee.org>.

Digital Object Identifier 10.1109/TVT.2011.2134876

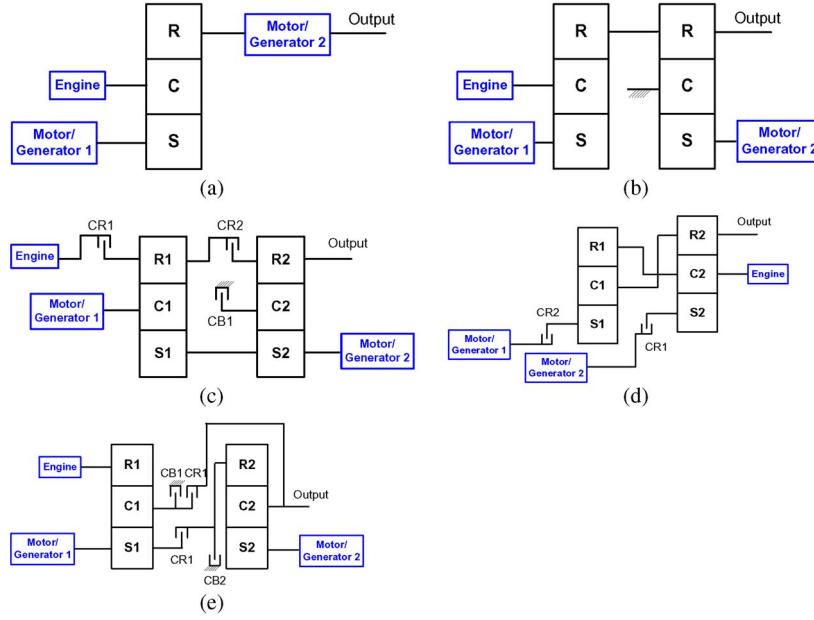


Fig. 1. Schematic of several existing EVT. (a) THS [3]. (b) Improved THS [6]. (c) Allison architecture [9]. (d) Renault architecture [10]. (e) Timken architecture [11].

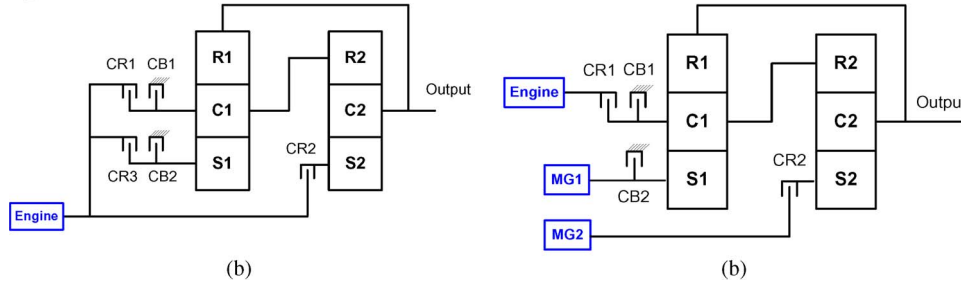


Fig. 2. Schematic of the proposed EVT. (a) Conventional four-speed AT. (b) Proposed EVT.

clutches (which are denoted CR), and two are braking clutches (which are denoted CB). The engine is the only power source.

The proposed EVT has two electric machines MG1 and MG2. Together with the engine, these three power sources are connected to the two planetary gearsets through CR1, CB2, and CR2, respectively. CR3 is used to change speed ratio in the conventional AT. However, in the EVT, speed ratio can be modulated by MG1 and MG2; therefore, CR3 is unnecessary and is eliminated. The EVT reuses some of the hardware of the conventional AT, including the planetary gearset topology and clutches, as shown in Fig. 2.

Compared with THS in Fig. 1(a), which is a typical clutchless EVT, the proposed EVT has four clutches, which is more complex. However, the hardware is derived from a conventional and popular four-speed AT; therefore, the reliability and cost are likely to be superior to EVTs that are newly designed. In addition, this paper will investigate the advantages of using clutches, which improves powertrain efficiency by reducing spin losses, extends life cycle, and optimizes efficiencies of the electric machines.

B. Operation Modes

The proposed EVT can realize both series and parallel operations. In the series mode, the engine can charge the battery through MG1 when CB1 and CB2 are open and CR1 is locked. MG2 can utilize the battery energy to drive the vehicle by engaging CR2. In the parallel mode,

the engine and the two motors drive the vehicle together through the 2-DoF planetary gearsets. Typically, the engine is set to operate in a high-efficiency region by regulating the speed and torque of the two electric machines.

Nine operation modes for the EVT-based SPHEV are described in Fig. 3. The operational modes are selected by engaging or disengaging the clutches and brakes.

CB2 and CR2 can be controlled to reduce the power losses at MG1 and MG2. When CB2 is locked, both the rotational speed and output torque of MG1 are zero, and therefore, the power loss of MG1 is also zero. When CR2 is open, MG2 is disconnected, and therefore, the power loss of MG2 is zero. When the energy management requires no power flow through MG1 or MG2, they neither have to work just for torque balance of the planetary gearsets nor rotate with the shafts. Thus, spin loss of the SPHEV is smaller, compared with that of a clutchless design.

III. MODELING

The EVT vehicle models are built in MATLAB/SIMULINK, and the control strategy is developed using the Stateflow toolbox. The top-level simulation model is shown in Fig. 4. T_{eng} , T_{MG1} , and T_{MG2} denote the output torque of the engines MG1 and MG2, respectively. ω_{eng} , ω_{MG1} , and ω_{MG2} denote their angular velocities. T_{EVT} stands for the output torque of the EVT, T_{BRK} is the braking torque provided

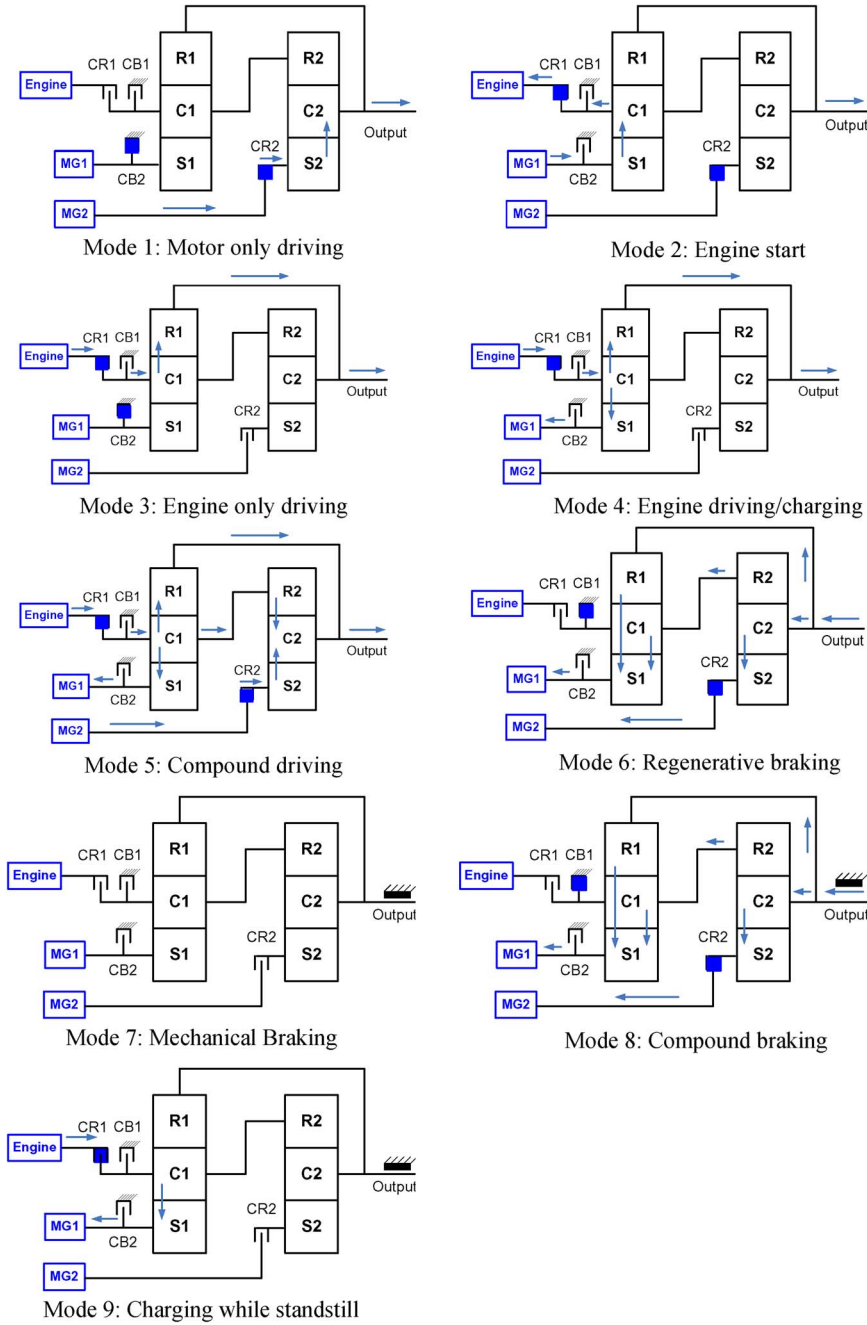


Fig. 3. Operation modes of SPHEV (■: engaged, □: disengaged). Mode 1: Motor-only driving. Mode 2: Engine start. Mode 3: Engine-only driving. Mode 4: Engine driving/charging. Mode 5: Compound driving. Mode 6: Regenerative braking. Mode 7: Mechanical Braking. Mode 8: Compound braking. Mode 9: Charging while standstill.

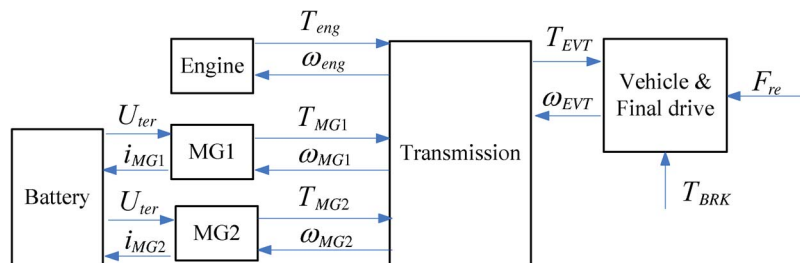


Fig. 4. Top-level structure of the vehicle model with EVT.

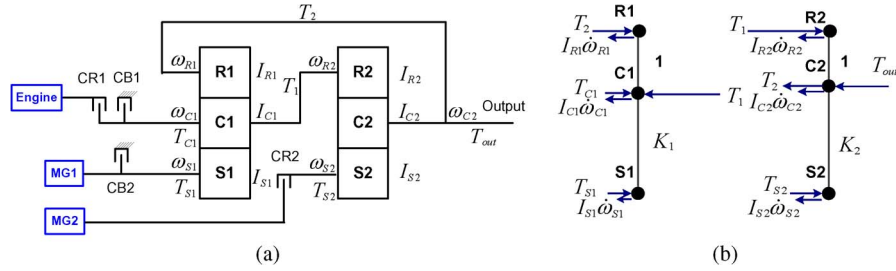


Fig. 5. Schematic and lever analogy of the EVT.

by the vehicle mechanical braking system, and ω_{EVT} stands for its angular velocity. U_{ter} is the battery terminal voltage. Since MG1 and MG2 are connected in parallel, the battery terminal voltages are the same for MG1 and MG2. I_{MG1} and I_{MG2} are the terminal bus currents of MG1 and MG2. F_{re} is the vehicle resistance force.

The derivations for the models of the vehicle, engine, electric motor, and battery are similar to those in [13]–[16]. In the following, we focus on the EVT model and the clutch model.

A. EVT Model

The schematic and the lever analogy of the EVT are shown in Fig. 5. For the first planetary gearset, I_{R1} , I_{C1} , and I_{S1} denote the inertia about the shafts of R1, C1, and S1, respectively. Whether the engine and MG1 contribute to the inertia depends on the status of the corresponding clutches. For example, the engine is part of I_{C1} when CR1 is engaged and CB1 is disengaged, etc. T_{C1} and T_{S1} denote the external torque applied to C1 and S1, respectively. ω_{R1} , ω_{C1} , and ω_{S1} denote the angular velocities of R1, C1, and S1, respectively. Similar definitions are applied to the second planetary gearset.

Since C1 is connected to R2, an interactional torque exists, which is denoted as T_1 . Similarly, the interactional torque between R1 and C2 is denoted as T_2 . T_{out} is the load torque, which is a counterforce of the EVT output torque T_{EVT} . To simplify the derivation, let K_1 denote the ratio of the ring gear teeth number to the sun teeth number of the first planetary gearset and K_2 denote the same ratio of the second planetary gearset.

Applying the lever analogy [4], the two planetary gearset are shown in Fig. 5(b). The mass of each node represents the inertia of the corresponding gear. Forces applied to each node represent the torques applied to the corresponding gear. Horizontal displacement of each node represents the magnitude of its angular velocity. By assuming the length between the carrier gear node and the ring gear node to be one, the length between the carrier gear node and the sun gear node is equal to the teeth number ratio K_i between the ring gear and the sun gear.

Each lever has one translational DoF and one rotational DoF. For the first lever, the equilibrium equation in terms of its translational DoF can be presented as follows:

$$T_{C1} + T_{S1} + T_2 - T_1 - I_{R1} \cdot \dot{\omega}_{R1} - I_{C1} \cdot \dot{\omega}_{C1} - I_{S1} \cdot \dot{\omega}_{S1} = 0. \quad (1)$$

Taking moment balance about C1, the equilibrium equation in terms of its rotational DoF can be derived as

$$T_{S1} \cdot K_1 - I_{S1} \cdot \dot{\omega}_{S1} \cdot K_1 - T_2 + I_{R1} \cdot \dot{\omega}_{R1} = 0. \quad (2)$$

Similarly, the equilibrium equations of the second lever are derived as follows:

$$\begin{aligned} T_1 + T_{S2} - T_{out} - T_2 - I_{R2} \cdot \dot{\omega}_{R2} \\ - I_{C2} \cdot \dot{\omega}_{C2} - I_{S2} \cdot \dot{\omega}_{S2} = 0 \end{aligned} \quad (3)$$

$$\begin{aligned} T_{S2} \cdot (1 + K_2) - I_{S2} \cdot \dot{\omega}_{S2} \cdot (1 + K_2) \\ - T_2 - T_{out} - I_{C2} \cdot \dot{\omega}_{C2} = 0. \end{aligned} \quad (4)$$

Here, ω_{R1} , ω_{C1} , ω_{S1} , ω_{R2} , ω_{C2} , and ω_{S2} are the six state variables in (1)–(4). They are subject to four kinematic constraints, i.e.,

$$\omega_{R1} = \omega_{C2}$$

$$\omega_{C1} = \omega_{R2}$$

$$K_1 \cdot \omega_{R1} + \omega_{S1} = (1 + K_1) \cdot \omega_{C1}$$

$$K_2 \cdot \omega_{R2} + \omega_{S2} = (1 + K_2) \cdot \omega_{C2}. \quad (5)$$

Therefore, there are only two independent state variables.

After eliminating the internal torques T_1 and T_2 , and choosing ω_{C1} and ω_{C2} as the independence variables, the following matrix equation can be derived:

$$\mathbf{T}_{cal} = \mathbf{A} \cdot \begin{bmatrix} \dot{\omega}_{C1} \\ \dot{\omega}_{C2} \end{bmatrix} \quad (6)$$

where (7) and (8), shown at the bottom of the page, hold.

Equation (6) calculates the effect of input torques on engine and vehicle speed. The speeds of the two electric machines can then be computed from (5).

B. Clutch Model

A simple clutch model is shown in Fig. 6, where T_{clu} denotes the torque transmitted by the clutch, T_{c_in} denotes the input torque of the

$$\mathbf{T}_{cal} = \begin{bmatrix} T_{C1} + T_{S1} + T_{S2} - T_{out} \\ T_{S2} \cdot (1 + K_2) - T_{S1} \cdot K_1 - T_{out} \end{bmatrix} \quad (7)$$

$$\mathbf{A} = \begin{bmatrix} I_{R2} + I_{C1} - I_{S2} \cdot K_2 + I_{S1} \cdot (1 + K_1) & I_{R1} + I_{C2} - I_{S1} \cdot K_1 + I_{S2} \cdot (1 + K_2) \\ -I_{S1} \cdot K_1 \cdot (1 + K_1) - I_{S2} \cdot (1 + K_2) \cdot K_2 & I_{S1} \cdot K_1^2 + I_{R1} + I_{C2} + I_{S2} \cdot (1 + K_2)^2 \end{bmatrix} \quad (8)$$

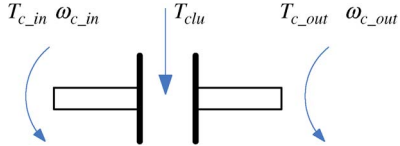


Fig. 6. Clutch model.

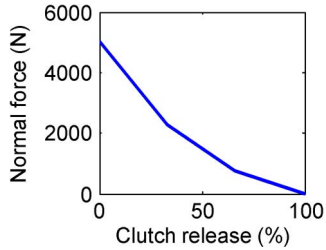


Fig. 7. Clutch normal force profile.

clutch driving shaft, T_{c_out} denotes the output torque of the clutch driven shaft, and ω_{c_in} and ω_{c_out} denote the rotational speeds of the clutch driving shaft and driven shaft, respectively.

A simple clutch model is shown in Fig. 6, where T_{clu} denotes the torque transmitted by the clutch, T_{c_in} denotes the input torque of the clutch driving shaft, T_{c_out} denotes the output torque of the clutch driven shaft, and ω_{c_in} and ω_{c_out} denote the rotational speeds of the clutch driving shaft and driven shaft, respectively.

There are three stages of the clutch, i.e., locked, slipping, and open. In the lock stage, the driving and driven plates of the clutch are locked with the same rotational speeds. In the slipping stage, the driving and driven plates have different rotational speeds. In the open stage, the driving and driven plates are not connected and can independently rotate. The governing equations of the output torque T_{c_out} in these three stages are given by

$$\begin{aligned}
 T_{c_out} &= T_{clu} = T_{c_in} && \text{when locked} \\
 T_{c_out} &= T_{clu} = \text{abs}(\mu \cdot P_{clu} \cdot R_{clu} \cdot N) \\
 &\quad \cdot \text{sign}(\omega_{c_in} - \omega_{c_out}) && \text{when slipping} \\
 T_{c_out} &= T_{clu} = 0 && \text{when open} \quad (9)
 \end{aligned}$$

where μ is the frictional coefficient of the clutch frictional plates, P_{clu} is the clutch normal force, R_{clu} is the equivalent radius of the plates, N is the number of frictional surfaces, and $\text{sign}(\cdot)$ is the signum function.

The clutch normal force varies along with the clutch release command, and the relations are shown in Fig. 7.

IV. ENERGY MANAGEMENT STRATEGY

The proposed energy management system consists of three modules: 1) torque requirement calculation; 2) mode decision; and 3) torque distribution, as shown in Fig. 8. The torque requirement calculation module outputs the required torque for the powertrain according to driver intention and vehicle status. The mode decision module selects the proper operation mode, and then, the torque distribution module distributes the optimal torque commands to the engine and the two motors.

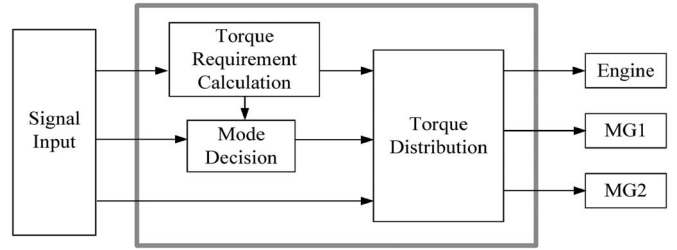


Fig. 8. Schematic of the energy management system.

A. Torque Requirement Calculation

Typically, the acceleration pedal and brake pedal are used to capture the driver intention and calculate the required torque [13]. An accurate driver intention model requires much calibration and a tracking-error feedback modulation.

This paper will investigate the economic performance of an SPHEV running on a predefined driving cycle. Because vehicle speed and road profile are given by the driving cycle, the required output torque of the EVT T_{req} can be directly derived from the vehicle longitudinal dynamics equation as follows, instead of a driver intention model:

$$\begin{aligned}
 T_{req} &= F_{tr} \cdot \frac{r_w}{I_f \eta_T} + T_{BRK} \\
 &= (F_r + F_g + F_{air} + m\delta v_h) \cdot \frac{r_w}{I_f \cdot \eta_T} + T_{BRK} \quad (10)
 \end{aligned}$$

where F_{tr} is the vehicle traction force, r_w is the rolling radius of the vehicle tire, i_f is the final drive ratio, η_T is the driveline efficiency, F_r is the rolling resistance, F_g is the slope resistance due to gravity, F_{air} is the aerodynamic drag force, m is the vehicle mass, δ is a lumped coefficient to incorporate the effect of rotational inertia, and v_h is the vehicle speed.

The EVT does not output torque in mechanical braking mode (mode 7); therefore, T_{req} is equal to zero, and the SPHEV is totally braked by T_{BRK} . In compound braking mode (mode 8) and charging while standstill mode (mode 8), the EVT and the mechanical braking system both affect the SPHEV dynamics; therefore, neither T_{req} nor T_{BRK} are not zero. In the other five modes, the mechanical braking system does not work, and therefore, T_{BRK} is equal to zero.

B. Mode Selection

An energy management controller is used to choose the appropriate mode from the nine available operation modes based on the torque requirement, vehicle states, and battery state of charge. Extensive studies of the power management strategy had employed techniques such as fuzzy logic or neural networks for estimation and control algorithm development [13]. Another approach is based on optimization methods [14], [15]. Additionally, many existing hybrid vehicles use rule-based control strategy because of the ease in handling changes in the operating mode. Rule-based control strategies are developed based on engineering intuition and simple analysis of component-efficiency tables [16].

In this paper, a rule-based control strategy is used to control the operation mode of the SPHEV. This control strategy uses the engine as a primary power source and the motors as the supplemental power source. The efficiency of the gasoline engine is high when the engine speed is in the range of $[\omega_{low} \ \omega_{up}]$ and when the engine torque is in the range of $[T_{e_low} \ T_{e_up}]$. The control strategy aims to operate in the high-efficiency range through seven rules. The flowchart shown

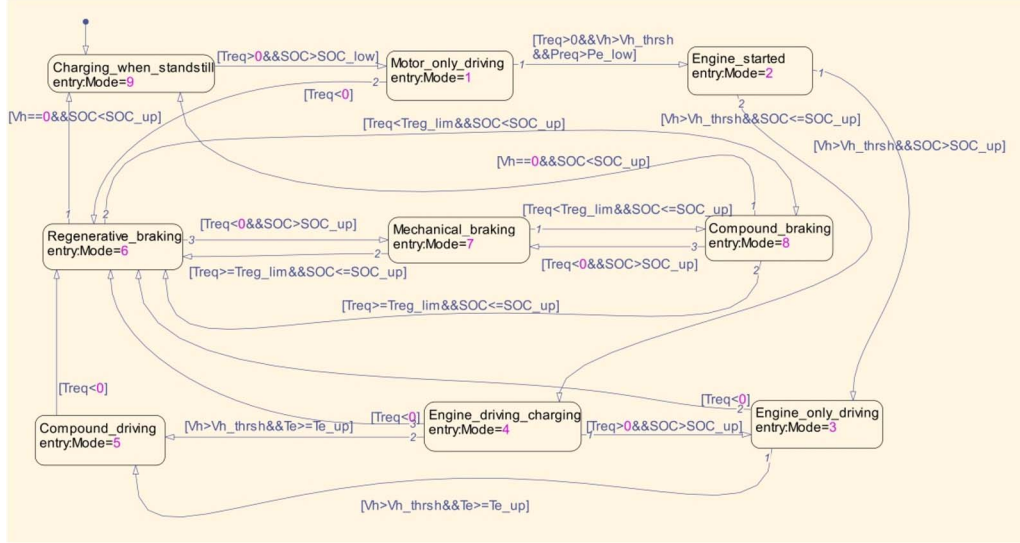


Fig. 9. Stateflow chart of the energy management controller.

in Fig. 9 depicts the overall implementation of the control strategies in the MATLAB Stateflow toolbox.

- 1) To avoid inefficient engine operations, the engine shuts off, and the electric motor supplies all driving torque (i.e., use mode 1) below a certain vehicle speed denoted by v_{h_thrsh} or below a certain power denoted by P_{e_low} , which is the product of T_{e_low} and ω_{e_low} .
- 2) The electric motor provides assistive torque if the required torque exceeds the maximum torque limit T_{e_up} of the engine high-efficiency area, that is, the SPHEV operates in the compound driving mode (mode 5). In this mode, the percentage of the engine torque is selected so that the engine operates in the high-efficiency region.
- 3) When the battery SOC drops below the upper limit denoted by SOC_{up} and the required torque does not exceed the maximum torque limit T_{e_up} of the high-efficiency region, the engine provides additional torque, which passes through MG1 to charge the battery. Thus, the SPHEV operates in the engine-driving/charging mode (mode 4) until SOC reaches SOC_{up} . The generator power is limited under the rated capacity of the battery to prevent battery damage.
- 4) When the required power is negative and SOC is below SOC_{up} , the regenerative braking mode (mode 6) is activated. Since the regenerative braking power is limited by the rated capacity of the battery, the regenerative braking torque denoted by T_{reg_lim} is also limited.
- 5) When the negative required torque is less than T_{reg_lim} and SOC is below SOC_{up} , the mechanical braking system provides the additional braking torque in compound braking mode (mode 8).
- 6) When SOC reaches SOC_{up} , regenerative braking is not preferred for battery durability consideration. When the required power is negative, the SPHEV operates in mechanical braking mode (mode 7).
- 7) To maintain battery capacity, the engine is allowed to charge the battery when the vehicle is at standstill. In this way, the battery can be always ready whenever the vehicle begins to run.

C. Torque Distribution

The relationship between the EVT input torques and output is specified in the dynamical equation (6). The torque distribution mod-

ule solves this equation based on measured data and predefined parameters.

On the right-hand side of (6), ω_{C2} corresponds to vehicle speed, which is measured. ω_{C1} relates to the speeds of the engine MG1 and MG2, depending on the status of clutches CB1 and CR1 shown in Fig. 5, i.e.,

$$\begin{aligned} \omega_{C1} &= \omega_{eng} && \text{when CB1 is open,} \\ & && \text{CR1 is locked} \\ \omega_{C1} &= 0 && \text{when CB1 is locked} \\ \omega_{C1} &= (\omega_{R1} \cdot K_1 + \omega_{S1}) / (1 + K_1) && \text{when CB1 and CR1} \\ & && \text{are open} \\ &= \omega_{R2} \\ &= (\omega_{C2} \cdot (1 + K_2) - \omega_{S2}) / K_2. \end{aligned} \quad (11)$$

Furthermore, ω_{S1} and ω_{S2} can be calculated as follows:

$$\begin{aligned} \omega_{S1} &= \omega_{MG1} && \text{when CB2 is open} \\ \omega_{S1} &= 0 && \text{when CB2 is locked} \end{aligned} \quad (12)$$

$$\begin{aligned} \omega_{S2} &= \omega_{MG2} && \text{when CR2 is locked} \\ \omega_{S2} &= 0 && \text{when CR2 is open.} \end{aligned} \quad (13)$$

In addition, ω_{R1} is equal to ω_{C2} according to (5).

The output speed of the proposed EVT ω_{C2} is proportionally related to the vehicle speed as follows:

$$\omega_{C2} = v_h \cdot r_w \cdot I_f. \quad (14)$$

Taking the derivative of ω_{C1} and ω_{C2} and plugging it into the right side of (6) yields the desired T_{cal} .

For the left side of (6), the entries of T_{cal} are related to T_{eng} , T_{MG1} , T_{MG2} , and T_{out} , depending on the status of the four clutches, i.e.,

$$\begin{aligned} T_{C1} &= T_{eng} && \text{when CB1 is open, and CR1 is locked} \\ T_{C1} &= 0 && \text{when CB1 and CR1 both are open} \end{aligned} \quad (15)$$

$$\begin{aligned} T_{S1} &= T_{MG1} && \text{when CB2 is open} \\ T_{S1} &= 0 && \text{when CB2 is locked} \end{aligned} \quad (16)$$

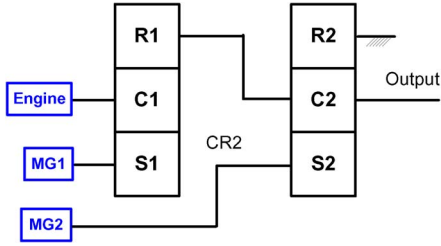


Fig. 10. Diagram of “Improved THS-like” EVT.

TABLE I
VEHICLE SPECIFICATIONS

Parameter	Value
gross mass m (kg)	1645
rolling radius r_w (m)	0.291
rolling resistance coefficient f	0.011
air resistance coefficient c_D	0.32
frontal area A_V (m ²)	1.746
final drive ratio i_f	3.905
driveline efficiency η_T (%)	99
engine maximum power P_{eng_max} (kW)	55
engine maximum speed ω_{eng_max} (rpm)	4700

$$T_{S2} = T_{MG2} \quad \text{when CR2 is locked}$$

$$T_{S2} = 0 \quad \text{when CR2 is open} \quad (17)$$

$$T_{out} = T_{req}. \quad (18)$$

Torque T_{req} can be calculated according to (10). T_{eng} , T_{MG1} , and T_{MG2} are to be modulated to satisfy the requirement specified in (6). If one of the three torque variables is given, then the other two can be uniquely computed from the two equations given in (6). The solutions for the nine operation modes are derived, respectively, in the Appendix.

V. SIMULATION AND ANALYSIS

The performance of the proposed SPHEV is demonstrated by comparing against an “Improved THS-like” vehicle, which uses two planetary gearsets without clutch but all the vehicle parameters are the same as the target vehicle studies in this paper. The diagram of the “Improved THS-like” EVT is shown in Fig. 10 [17]. The second planetary gearset is considered as a reduction gear, because its ring gear is fixed. The connections of the ring gear and carrier gear are different from those of the improved THS, as shown in Fig. 1(b). By calculation, the MG2 torque range of the improved THS is wider than that of the “Improved THS-like” EVT under the same output requirement. This paper uses the same MG2 to justify the comparison; therefore, the “Improved THS-like” EVT is considered as the benchmark, instead of the improved THS. The way to connect the engine MG1 and MG2 of the “Improved THS-like” vehicle is the same as that of the proposed SPHEV. The New European Driving Cycle (NEDC) comprehensive driving cycle, which consists of four identical urban cycles and one extra-urban cycle with frequent start/stop, is used to assess the vehicle performance [18].

A. Specifications and Control Parameters

To reduce fuel consumption, the engine for the proposed SPHEV is downsized from 80 to 57 kW. The engine is augmented by MG1

TABLE II
EVT SPECIFICATIONS

Parameter	Value
Power of MG1 P_{MG1_max} (kW)	15
Maximum speed of MG1 ω_{MG1_max} (rpm)	6000
Maximum Power of MG2 P_{MG2_max} (kW)	30
Maximum speed of MG2 ω_{MG2_max} (rpm)	7000
Battery capacity Q_0 (A-h)	260
Voltage of battery pack U_{OC} (V)	304
Battery cell internal resistance (charge) R_i (Ohm)	0.0197
Battery cell internal resistance (discharge) R_i (Ohm)	0.0269
Planetary gearset 1 teeth number ratio K_1	1.842
Planetary gearset 2 teeth number ratio K_2	2.48
Moment of inertia of the first sun gear I_{P_S1} (kg·m ²)	0.00015
Moment of inertia of the first carrier gear I_{P_C1} (kg·m ²)	0.00018
Moment of inertia of the first ring gear I_{P_R1} (kg·m ²)	0.00020
Moment inertia of the second sun gear I_{P_S2} (kg·m ²)	0.00015
Moment of inertia of the second carrier gear I_{P_C2} (kg·m ²)	0.00017
Moment of inertia of the second ring gear I_{P_R2} (kg·m ²)	0.00020
Moment of inertia of the engine I_{eng} (kg·m ²)	0.13
Moment of inertia of MG1 I_{MG1} (kg·m ²)	0.22
Moment of inertia of MG2 I_{MG2} (kg·m ²)	0.30

TABLE III
PARAMETERS OF THE RULE-BASED ENERGY MANAGEMENT CONTROLLER

Parameter	Value
Engine speed range in high efficiency region $[\omega_{low} \ \omega_{up}]$ (rpm)	[1000 3000]
Engine torque range in high efficiency region $[T_{e_low} \ T_{e_up}]$ (Nm)	[60 100]
High efficiency SOC range $[SOC_{low} \ SOC_{up}]$ (%)	[44 55]
Maximum limit of regenerative braking torque T_{reg_lim} (Nm)	300
Vehicle speed threshold for mode 2 v_{h_threh} (km/h)	20

and MG2, which have the maximum power of 15 and 30 kW, respectively. A lithium iron phosphate battery is used as the energy storage system.

Specifications of the vehicle and EVT are listed in Tables I and II, respectively. The control parameters in Fig. 9 are selected as shown in Table III.

B. Simulation Results

The engine, MG1, MG2, battery, and vehicle parameters of the proposed SPHEV and the “Improved THS-like” vehicle are the same. The two vehicles basically use the same rule-based control strategy. They differ in the calculations of torque distribution due to their different mechanisms. The torque distribution for the proposed SPHEV

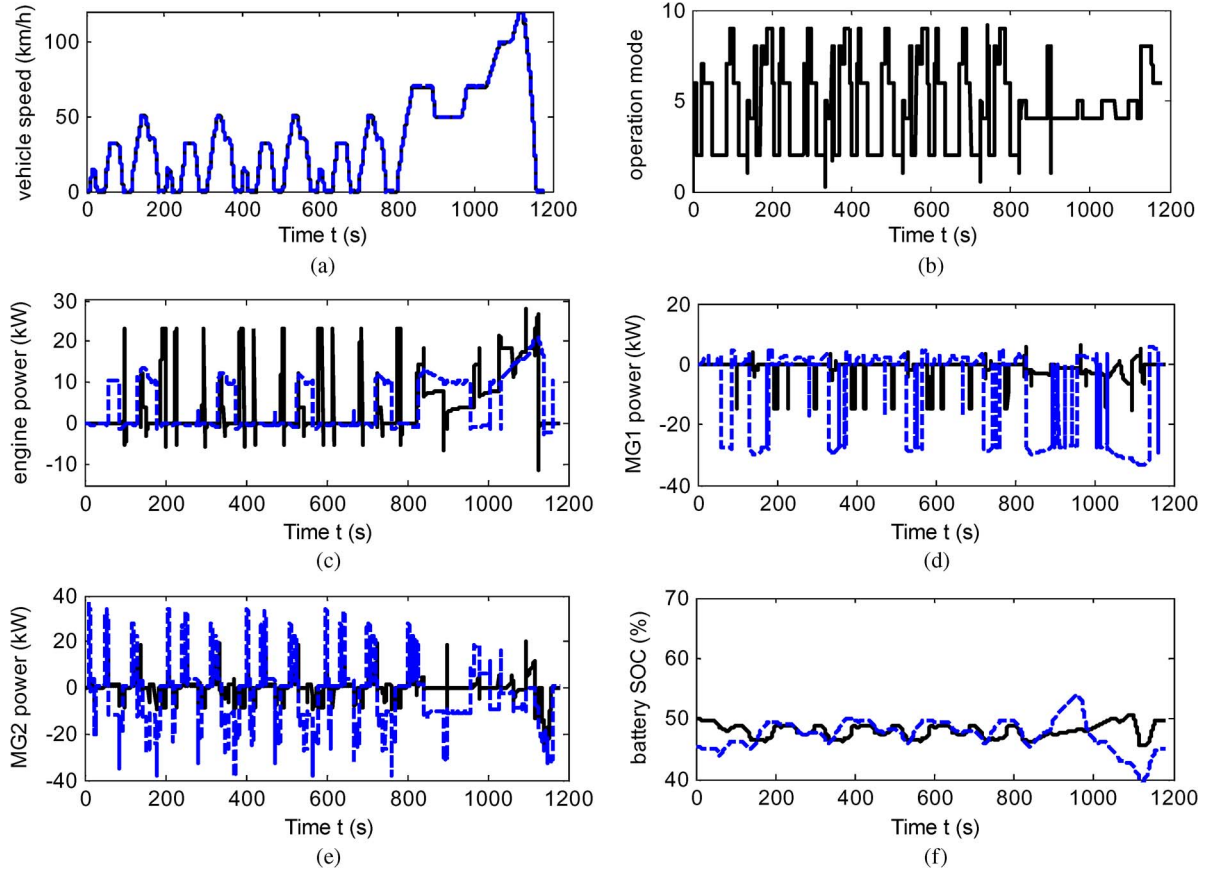


Fig. 11. Simulation results of NEDC. (a) Vehicle speed. (b) Operation mode. (c) Engine power. (d) MG1 power. (e) MG2 power. (f) Battery SOC.

is given in Section IV-C, and that for the “Improved THS-like” vehicle is calculated based on the fundamental torque and speed formulas of planetary gearsets, which are applied to several EVT with one or more planetary gearsets [14], [15].

In Fig. 11, the vehicle speed, operation mode, engine power, MG1 power, MG2 power, and *SOC* of battery are illustrated. The black solid line represents the results of the proposed SPHEV, and the blue dashed line represents those of the “Improved THS-like” vehicle.

Due to nonlinear stick-slip friction characteristics, the clutch engagement and disengagement are carefully controlled; otherwise, serious transient vibration may occur during mode transitions of the studied SPHEV. A model reference control, using angular velocities as feedbacks, is applied to achieve smooth running [19].

It can be seen from Fig. 11(b) that eight of the nine EVT modes are actuated. The only mode not used is mode 3 (engine-only driving). Because the battery *SOC* is reduced in mode 1 of motor-only driving, the battery needs to be charged when the engine is commanded to drive the vehicle; thus, the mode 4 of engine driving/charging is applied. Only when the battery *SOC* reaches its maximum limit can mode 3 be applied. However, before *SOC* reaches the maximum limit, the required engine torque T_{eng} exceeds the maximum torque in the high-efficiency area. Mode 5 (compound driving) is thus used.

Fig. 11(c) shows that much negative power occurs in the engine of the “Improved THS-like” vehicle. When only MG2 is driving the vehicle, the engine spins along with the carrier gear, resulting in higher spin losses. This spin loss does not occur in the proposed SPHEV, because clutch CR1 is open and the engine is at rest when MG2 is solely driving the vehicle. The accumulative rest time of the power devices in the proposed SPHEV is given in Table IV. During the 1200-s running time of the NEDC simulation, the engine rests for

TABLE IV
ACCUMULATIVE REST TIME OF THE ENGINE, MG1,
AND MG2 IN THE PROPOSED SPHEV

Power Device	Rest Time (s)	Percentage of the NEDC Running Time (%)
Engine	496.25	42.05
MG1	197.02	16.70
MG2	198.20	16.80

496.25 s, which is 42.05% of the total running time. That is, the engine stops working for almost half of the running time; therefore, the engine-involved spin loss is effectively reduced.

It can be seen from Fig. 11(d) and (e) that the intervals with zero power of MG1 and MG2 in the proposed SPHEV are much more than that in the “Improved THS-like” vehicle. In the proposed SPHEV, the open or lock operations of the clutches allow efficient usages of the electric machines. Table I shows that MG1 and MG2 cumulatively rest for 197.02 and 198.20 s in the NEDC running, respectively. The percentage data indicate that they stop working for about one fifth of the total running time, which can effectively extend their life cycle. However, in the “Improved THS-like” vehicle, the electric machines continuously rotate. When only the engine is driving the vehicle, MG1 provides a balance torque on the sun gear of the first planetary gearset, which means more power losses through MG1, and MG2 spins along with the sun gear of the second planetary gearset, which results in spin loss. When only MG2 is driving the vehicle, MG1 spins along with the sun gear, which means higher spin loss.

The operating points of the engines in both hybrid vehicles are shown in Fig. 12. The engine operating points concentrate in the

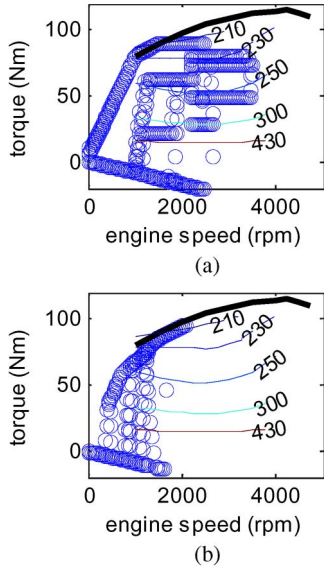


Fig. 12. Engine operating points. (a) Proposed SPHEV results. (b) “Improved THS-like” vehicle results.

high-efficiency region. However, there are some points with negative torque, which indicate engine braking. For the proposed SPHEV, negative engine torque occurs in three transient cases: 1) When the SPHEV transits from Motor-only driving mode (Mode 1) to Compound driving mode (Mode 5), the engine is started from zero speed. Before the engine can produce positive torque, its torque is negative because of inertia and friction. 2) When the SPHEV transits from Compound driving mode (Mode 5) to braking modes (Modes 6, 7, and 8), the engine speed decreases to zero without fuel supply; therefore, negative torque occurs because of friction. 3) When SOC reaches SOC_{up} in Charging while standstill mode (Mode 9), the engine stops fuel supply. The transient process from an engine speed to zero results in negative torque because of friction. In addition, Fig. 12(a) shows many operating points below contour line 250 g/kWh, which is not in the high-efficiency region. These points are in Engine-only driving mode (Mode 3) when SOC is low. They expose a deficiency of the current control rule and may disappear by a well-tuned optimal control method. For the “Improved THS-like” vehicle, the engine always spins with the carrier of the first planetary gearset; therefore, negative engine torque may occur. From Fig. 12, there are more points with negative torque in the “Improved THS-like” vehicle than in the proposed SPHEV, i.e., more losses.

In addition, Fig. 12(a) shows that some operating points in the proposed SPHEV have torque below 60 N · m, which is out of the efficiency range. These points correspond to the engine-driving/charging mode. When the load is low and the battery SOC is high, the required engine torque is low, resulting in inefficient engine operations. The rule-based control strategy may need further optimization by either increasing the vehicle speed threshold v_{h_thrsh} for mode 2 (motor-only driving) or reconfiguring the battery.

The operating points of MG1 and MG2 are shown in Figs. 13 and 14, respectively. The operating points of MG1 in the first and third quadrants correspond to motoring. The points in the second and fourth quadrants correspond to generating. In the “Improved THS-like” vehicle, many operating points near the horizontal axis mean that the electric machines are spinning at low power. The proposed EVT avoids spin loss by using the clutches. In addition, the MG2 maximum speed of the “Improved THS-like” vehicle is up to 14 700 r/min, which approximately closes to the publicized data 13 900 r/min in [6]. The extrawide range of MG2 exposes the control inflexibility of

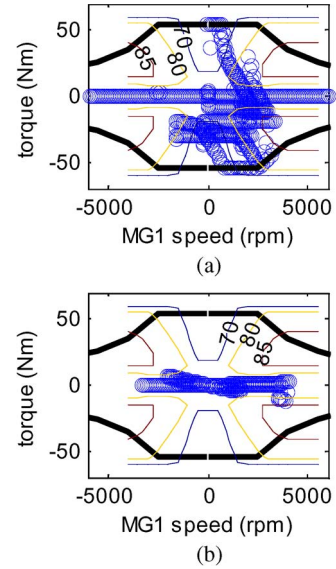


Fig. 13. MG1 operating points. (a) Proposed SPHEV results. (b) “Improved THS-like” vehicle results.

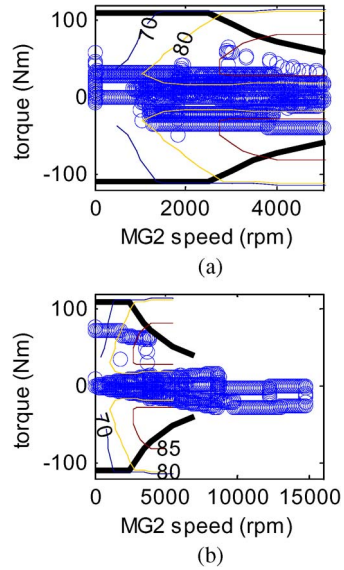


Fig. 14. MG2 operating points. (a) Proposed SPHEV results. (b) “Improved THS-like” vehicle results.

the “Improved THS-like” EVT structure and implies big challenges of manufacture, stability, and cost for the electric machines.

Over the whole NEDC cycle, the proposed SPHEV achieves a fuel consumption of 55.33 mpg, whereas that of the “Improved THS-like” vehicle is 52.38 mpg. In other words, the fuel consumption of the EVT-based SPHEV is reduced by 5.62%. If the rule-based energy management is optimized, e.g., by dynamics programming, the fuel consumption of the proposed SPHEV might be further improved.

VI. CONCLUSION

An EVT combining two planetary gearsets and four clutches has been proposed in this paper for an SPHEV. The EVT proposed here is very similar to the planetary gearsets used in several existing four-speed ATs and can have nine operation modes, i.e., motor-only

driving, engine started, engine-only driving, engine driving/charging, compound driving, regenerative braking, mechanical braking, compound braking, and charging while standstill mode. A model of the EVT based SPHEV has been developed in the MATLAB/SIMULINK environment. A rule-based energy management control strategy using the efficiency maps of the components for estimating the power performance of the SPHEV has been presented.

The fuel consumption of the proposed SPHEV is 5.62% lower than that of the "Improved THS-like" vehicle, which indicates the fuel economy potential of this concept. One reason is that spin losses can be avoided by using the clutches.

The life cycle of the electric machines is expected to be effectively extended, because the open or lock operations of the clutches allow efficient usages in the proposed SPHEV. In addition, the speed of the electric machines is effectively confined to an acceptable range, compared with that in the "Improved THS-like" vehicle, which implies ease of manufacture, good sustainability, and low cost.

REFERENCES

- [1] C. C. Chan, "The state of the art of electric, hybrid, and fuel cell vehicles," *Proc. IEEE*, vol. 95, no. 4, pp. 704–718, Apr. 2007.
- [2] M. J. Hoeijmakers, "The electric variable transmission," *IEEE Trans. Ind. Appl.*, vol. 42, no. 4, pp. 1092–1100, Jul./Aug. 2006.
- [3] R. H. Staunton, C. W. Ayers, L. D. Marlino, J. N. Chiasson, and T. A. Burress, "Evaluation of 2004 Toyota Prius hybrid electric drive system," U.S. Dept. Energy Freedom CAR Vehicle Technol., Washington, DC, ORNL/TM-2006/423, 2006.
- [4] H. Benford and M. Leising, "The lever analogy: A new tool in transmission analysis," presented at the Soc. Automotive Eng. Transaction, Warrendale, PA, 1981, SAE Paper 810102.
- [5] M. Ehsani, Y. Gao, and J. M. Miller, "Hybrid electric vehicle: Architecture and motor drives," *Proc. IEEE*, vol. 95, no. 4, pp. 719–728, Apr. 2007.
- [6] A. Takasaki, T. Mizutani, K. Kitagawa, T. Yamahana, K. Odaka, T. Kuzuya, Y. Mizuno, and Y. Nishikawa, "Development of new hybrid transmission for 2009 Prius," in *Proc. EVS24 Int. Battery, Hybrid Fuel Cell Elect. Veh. Symp.*, Stavanger, Norway, 2009.
- [7] J. D. Wishart, Y. Zhou, and Z. Dong, "Review, modelling and simulation of two-mode hybrid vehicle architecture," in *Proc. ASME Int. Des. Eng. Tech. Conf. Comput. Inf. Eng. Conf.*, Las Vegas, NV, 2007.
- [8] M. Cipek, J. Deur, and J. Petrić, "Bond graph modeling and analysis of series-parallel hybrid electric vehicle transmissions," presented at the Soc. Automotive Eng. World Congr. Exh., Detroit, MI, 2010, SAE Paper 2010-01-1309.
- [9] M. R. Schmidt, "Two-mode, input-split, parallel, hybrid transmission," U.S. Patent 5 558 588, Sep. 24, 1996.
- [10] A. Villeneuve, "Dual mode electric infinitely variable transmission," in *Proc. Int. CVT Hybrid Transm. Congr.*, Davis, CA, 2004.
- [11] X. Ai, T. Mohr, and S. Anderson, "An electromechanical infinitely variable speed transmission," presented at the Soc. Automotive Eng. World Congr. Exh., Detroit, MI, 2004, SAE Paper 2004-01-0354.
- [12] T. S. Birch and C. Rockwood, *Automatic Transmission & Transaxles*. Englewood Cliffs, NJ: Prentice-Hall, 2009.
- [13] W. Xiong, Y. Zhang, and C. Yin, "Optimal energy management for a series-parallel hybrid electric bus," *Energy Convers. Manage.*, vol. 50, no. 7, pp. 1730–1738, Jul. 2009.
- [14] Y. Zhang, H. Lin, B. Zhang, and C. Mi, "Performance modeling and optimization of a novel multi-mode hybrid powertrain," *Trans. ASME, J. Mech. Des.*, vol. 128, no. 1, pp. 79–89, Jan. 2006.
- [15] J. Liu and H. Peng, "Modeling and control of a power-split hybrid vehicle," *IEEE Trans. Control Syst. Technol.*, vol. 16, no. 6, pp. 1242–1251, Nov. 2008.
- [16] K.-B. Sheu, "Simulation for the analysis of a hybrid electric scooter powertrain," *Appl. Energy*, vol. 85, no. 7, pp. 589–606, Jul. 2008.
- [17] [Online]. Available: http://en.wikipedia.org/wiki/Hybrid_Synergy_Drive
- [18] O. Bitsche and G. Gutmann, "Systems for hybrid cars," *J. Power Sources*, vol. 127, no. 1/2, pp. 8–15, Mar. 2004.
- [19] L. Chen, G. Xi, L. Luo, and C. Yin, "Improve engagement performance for automated clutch using model referenced adaptive controller," *J. Syst. Simul.*, vol. 21, no. 16, pp. 5102–5104, 2009.

On Efficient Processing of Continuous Historical Top- k Queries in Sensor Networks

Jie Cheng, Hongbo Jiang, *Member, IEEE*,
Jiangchuan Liu, *Senior Member, IEEE*, Wenyu Liu, *Member, IEEE*,
and Chonggang Wang, *Senior Member, IEEE*

Abstract—The top- k query has long been an important topic in computer science. Efficient implementation of top- k queries is the key for information searching. In this paper, we develop the Efficient algorithm for the Continuous Historical Top- k (ECHT) extraction, which is a novel algorithm that can effectively process the continuous historical top- k query. A simple top- k extraction algorithm based on aggregation is used for user query processing, and two additional steps on the filter setting by which individual nodes do not have to report all their readings are proposed to further reduce communication cost. To the best of our knowledge, this is the first work for continuous historical top- k query processing in sensor networks, and our simulation results show that our schemes can reduce the total communication cost by up to two orders of magnitude, as compared with the centralized scheme or a straightforward extension from the previous top- k algorithm on a continuous monitoring query.

Index Terms—Algorithm/protocol design, sensor networks, top- k extraction.

I. INTRODUCTION

As energy conservation is crucial to the prolonged lifetime of a sensor network [1], many approaches [2], [3] have been explored, with particular attention to aggregate query processing. Among all those aggregates, the top- k query is crucial for many applications such as environment monitoring, network management, and biology analysis. Previous studies strive to propose energy-efficient processing approaches for the top- k query such that the list of k highest (or lowest) sensor readings is retrieved.

For many applications, users may want to continuously extract or aggregate data such as top- k results from sensor networks for later analysis. For example, one question posed by the sink could be "what is the average speed of sensor nodes for detecting vehicle speed whose readings are the lowest top- k within the past 1 hour?" In this case, if the sink receives most of the top-100 results from the same node (or its neighbors), this area where this node is located is possibly suffering from traffic congestion. Despite its importance, unfortunately, none of previous works have been done on the *continuous historical top- k extraction* problem in sensor networks. The "monitoring" top- k query

Manuscript received August 30, 2010; revised January 2, 2011 and February 6, 2011; accepted April 18, 2011. Date of publication April 29, 2011; date of current version June 20, 2011. This work was supported in part by the National Natural Science Foundation of China under Grant 60803115, Grant 60873127, Grant 60903096, and Grant 61073147; by the National Natural Science Foundation of China and Microsoft Research Asia under Grant 60933012; by the Youth Chenguang Project of Wuhan City under Grant 201050231080; by the Scientific Research Foundation for the Returned Overseas Chinese Scholars (State Education Ministry); and by the Program for New Century Excellent Talents in University (State Education Ministry). The review of this paper was coordinated by Prof. A. Jamalipour.

J. Cheng, H. Jiang (Corresponding author), and W. Liu are with Department of Electronics and Information Engineering, Wuhan National Laboratory for Optoelectronics, Huazhong University of Science and Technology, Wuhan 430074, China (e-mail: hongbojiang2004@gmail.com).

J. Liu is with the School of Computing Science, Simon Fraser University, Burnaby, BC V5A 1S6, Canada.

C. Wang is with InterDigital Communications, USA.

Color versions of one or more of the figures in this paper are available online at <http://ieeexplore.ieee.org>.

Digital Object Identifier 10.1109/TVT.2011.2148203